Experimental and Analytical Study of an Axisymmetric Thrust Augmentor

Harry R. Skoblenick*
Queen's University, Kingston, Ont., Canada
and
Philip G. Hill†
University of British Columbia, Vancouver, B.C., Canada

An axisymmetric thrust augmentor of area ratio 24:1 and thrust augmentation ratio 1.45 has been built and tested. Measurements were made of augmentor thrust and mass flow and of velocities, wall pressures, and wall shear stresses within the duct. The experimental data were compared with the results of a finite-difference mathematical model of the flowfield, which incorporated an eddy viscosity method of calculating turbulent shear stresses. With adjustment of eddy viscosity parameters, the mathematical flow model was shown to be capable of a close simulation of the flowfield and to provide a good description of the nearly separating flow in the diffuser. Predicted thrust was within 5% of measured thrust, for the same exit pressure, making allowance for losses in the nozzles. Data from a partially blocked exit test provided further evidence of the ability of the mathematical model to represent the internal flowfield.

Nomenclature

a = speed of sound
A^* = nozzle throat area
d = diameter, nozzle exit or Preston tube
d^* = dimensionless Preston tube diameter $U_\tau d/\nu_w$
D = duct diameter, cross section or throat
k_e = mixing coefficient (see Fig. 2)
$\dot{m}$ = mass flow rate
M = Mach number
M_τ = friction Mach number U_τ/a_w
P = static pressure
P_0 = stagnation pressure
ΔP_p = difference between local wall static pressure and Preston tube pressure
P_{is} = isentropic static pressure at nozzle exit plane
R = gas constant, duct radius
T_0 = stagnation temperature
T_{aug} = augmentor system thrust
T_{duct} = augmentor duct thrust
T_n = nozzle thrust with augmentor duct removed
T_{is} = choked isentropic nozzle thrust with convergent nozzle and ambient back pressure
u = axial component of velocity at a particular point in a cross section
U = axial velocity outside boundary layer
U_τ = wall friction velocity $\sqrt{(\tau_w/\rho_w)}$
U_ℓ = centerline velocity
V = air velocity
V_{is} = isentropic flow velocity at nozzle exit plane
γ = ratio of specific heats
δ^* = displacement thickness
Δy = distance from mixing section wall
ν = kinematic viscosity
ϵ = eddy viscosity
ν_T = total effective viscosity, $= \nu + \epsilon$
τ = shear stress
ρ = fluid density
ϕ = thrust augmentation coefficient T_{aug}/T_n
η_T = nozzle thrust coefficient T_n/T_{is}
η_m = nozzle mass coefficient $\dot{m}_1/\dot{m}_{is}$

Subscripts

0 = reference condition
1 = primary stream
2 = secondary stream
atm = atmosphere
is = isentropic
w = wall condition

Superscript

$(\bar{\ })$ = time-averaged value

Received June 18, 1976; revision received Jan. 26, 1977.
Index categories: Airbreathing Propulsion; Powerplant Design; Nozzle and Channel Flow.
*Research Assistant.
†Professor of Mechanical Engineering.

I. Introduction

FIGURE 1 shows a schematic view of a static thrust augmentor. It indicates the high-speed jet whose turbulence entrains secondary air, drawing it into the low-pressure throat region, or mixing zone. On leaving this zone, the flow is nonuniform but capable of pressure rise in the diffuser to ambient static pressure. At the diffuser exit, the total momentum flux is higher than that of the nozzle alone so that the duct enclosing the flow augments the nozzle thrust (as long as the wall shear stresses are not excessive).

One-dimensional flow analysis shows that thrust augmentation ϕ improves with the use of a diffuser and is quite dependent upon the degree of uniformity of the exit flow. Figure 1 demonstrates the results of Whittley,[1] showing the importance of the diffuser area ratio and the augmentor thrust-to-nozzle exit area ratios. The mixing coefficient K_e (defined in Fig. 1) is an indicator of the uniformity of the flow at the diffuser exit. A value of K_e of 1 signifies a completely uniform profile; real flows have K_e greater than 1. Increasing K_e from 1.0 to 1.2 can decrease the thrust by as much as 15%. Figure 1 shows the importance of the diffuser in contributing to the thrust augmentation coefficient. The results of Whittley[1] are ideal in that they neglect wall shear stresses and the possibility of flow separation. These factors subtract substantially from the ideal values of ϕ shown in Fig. 1.

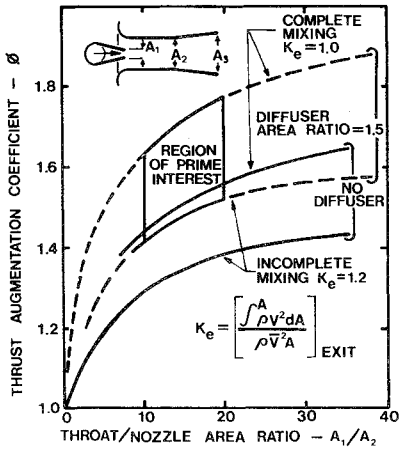

Fig. 1 Theoretical trends in static augmentation.[1]

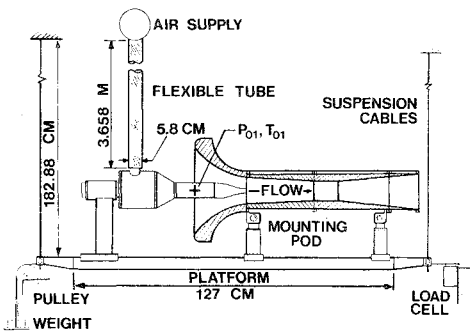

Fig. 2 Mounting and suspension of the thrust augmentor.

The duct in a practical device should be long enough to permit adequate mixing but not so long that internal frictional losses predominate. The diffuser should be short (for low weight) but not so short that flow breakdown (separation) occurs. These considerations and others suggest the need for a mathematical model of predicting the flowfield (including the wall shear stresses) for any augmentor configuration, at least in the absence of separation.

Prior experimental work on thrust augmentor models is reported in Refs. 2-4. Cheng et al.[2] measured thrust augmentation with a straight-pipe duct (no diffuser). They found thrust augmentation to be quite sensitive to pipe length-diameter ratio, duct-to-nozzle area ratio, and nozzle location but did not obtain velocity profiles or wall pressures and shear stresses. In the absence of a diffuser, they did not encounter flow separation. Fancher[3] measured thrust augmentation ratio with a plane-symmetric augmentor of variable secondary-to-primary area ratio and variable diffuser ratio. His results showed that ϕ increases both with secondary-to-primary area ratio and with diffuser ratio (up to a value of about 1.6:1). A special feature of Fancher's work was the use of a "hypermixing" nozzle: a two-dimensional nozzle with a regular array of slotted segments alternately on upper and lower edges of the nozzle walls. By measuring centerline velocity, Fancher showed the effectiveness of this geometry in enhancing jet mixing in the upstream region of the augmentor. Quinn[4] measured thrust augmentation ratio as a function of diffuser area ratio, mixing section length, and diffuser length. He also used hypermixing nozzles in a plane-symmetric duct. By means of end-wall blowing, he was able to increase ϕ in one case from 1.6 to 2.0.

Detailed experimental data on the flowfield internal to thrust augmentors have not been published, although corresponding information is available to some extent from studies on ejectors.[5-15] The results of these studies include pressure and velocity information for fairly long ejectors and have confirmed the validity of finite-difference flow models in predicting the wall pressures and centerline velocity decay. However, more experimental information is required to assess the feasibility of models for nearly separating flow in short thrust augmentors. The purpose of this work was to provide data on wall shear stresses, in addition to velocity and pressure information, and to apply a finite-difference calculation method to determine the predictability of nearly separating augmentor flow.

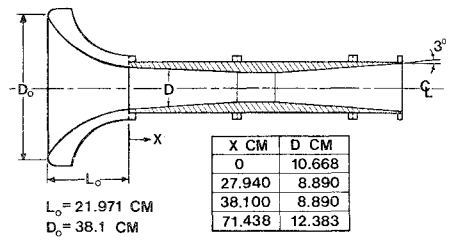

X CM	D CM
0	10.668
27.940	8.890
38.100	8.890
71.438	12.383

Fig. 3 Augmentor duct geometry.

II. Apparatus

Figure 2 shows the suspension of the experimental augmentor with provision for measurement of thrust on the mounting frame. Figure 3 provides the geometry of the augmentor. Further details on the test augmentor geometry are given in Ref. 5. A value of 2:1 was selected as the diffuser exit-to-throat area ratio, to enable a reasonable pressure recovery to take place in a reasonable length without flow separation. The duct was designed for gradual convergence before the throat, to discourage wall boundary-layer separation while the exit flow was throttled. The nozzle was concentric with the longitudinal axis of the duct and positioned with its exit at the inlet of the conically converging section. The nozzle exit area of 0.399 in.^{2} (2.57 cm^2) was chosen to provide sonic flow with the compressor operating near maximum capacity. The duct inlet section has a contraction ratio of 13:1.

The duct throat-to-nozzle exit area ratio was chosen as 24:1, somewhat higher than the range of interest indicated by Fig. 1 (i.e., with area ratios ranging from 10 to 20). Given the limitations in the nozzle exit area already mentioned, it was desirable to make the duct-to-nozzle area ratio as large as possible to facilitate measurements within the duct. With an area ratio of 24:1, the duct throat diameter was 3.5 in. (8.9 cm). This allowed adequate room for total pressure-tube surveys without undue interference between probe and flow.

III. Measurements

Primary flow stagnation temperatures were measured, using copper-constantan thermocouples, at two locations: one upstream of the primary flow meter, and the other midway between the plenum chamber and the nozzle exit plane (see Fig. 2). The primary flow stagnation pressure P_{01} was calculated from measurements of wall static pressure P_1 (measured midway between the nozzle and the plenum chamber; see Fig. 2), the cross-sectional area of the extension tube, the primary flow rate, and the primary flow stagnation temperature.

The primary mass flow rate was obtained by measuring the static pressure drop across a British standard 1042 orifice plate, the static wall pressure at a station upstream of the meter, the line stagnation temperature, and using the B.S. 1042 calibration curves. The total flow rate $\dot{m}_1 + \dot{m}_2$ was evaluated by numerical integration (at various sections of the duct) of velocities and densities determined from measured pressures (obtained from static taps and an impact pressure tube) and measured stagnation temperatures. Secondary and primary stagnation temperatures were within 1% of each other. Since swirl and streamline curvature effects were negligible, the static pressure $\bar{P}$ was approximated closely by

the local wall static pressure $\bar{P}_w$. The impact probe was square-nosed with tip diameter 0.042 in. (0.107 cm).

Inserting the impact tube into the flow changed the downstream wall static pressures by as much as 5% of the difference between wall static and atmospheric pressure. This was particularly noticeable in the throat region when traverses were made in the first section of the duct. These changes were due principally to the probe drag and blockage effects on the flow. Probe cross-sectional area accounted for as much as 1% loss in the throat cross-sectional area. Wall static pressures used for obtaining the radial profiles of velocity were recorded before and after the probe was inserted into the test section. At most, the static pressure fluctuation would account for 1% error in velocity measurements. Agreement between values of $\dot{m}_1+\dot{m}_2$ calculated at various test sections was within ±2.4%.

The platform to the augmentor system was suspended in a frame by four separate cables (see Fig. 2). Thrust was measured with a thermally compensated load cell capable of detecting a peak thrust of ±25 lb (111 N) with a maximum beam deflection of only ±0.005 in. (0.013 cm). Three thrust measurements were made from the platform: thrust on the nozzle alone, thrust on the augmentor system, and thrust on the duct alone. The thrust on the nozzle alone was measured with the augmentor duct removed from the platform. The thrust on the complete augmentor system was measured with the nozzle and duct fastened to the platform. The thrust on the duct alone was measured with the nozzle mounting pad removed from the platform and fastened to an extension of the frame surrounding the platform. Operating the nozzle under pressure, but with a blocked exit, showed that the flexible tube had no effect on measured thrust.

The shear stress along the duct wall was determined experimentally by the use of Preston tubes and the calibration formula of Bradshaw,[16] which is in the form

$$\Delta P_P/\tau_w = f_i[d^*] + f_c[d^*, M] \qquad (1)$$

The dimensionless parameter $M_\tau = U_\tau/a_w$ (the "friction Mach number") is a measure of compressibility effect. The calibration is valid for $50 < d^* 1000, 0 < M_\tau < 0.1$.

The accuracy to which the skin friction can be evaluated is limited by the accuracy with which ΔP_p can be measured. To determine the effect of Preston tube diameter on the skin friction approximation, three tubes were used, of 0.125-, 0.062-, and 0.021-in. o.d. (0.318, 0.157, and 0.053 cm) and inside-to-outside diameter ratios of about 0.6. Figure 4 shows the geometry of the Preston tubes.

In all of the tests using the Preston tubes, the compressibility correction used by Bradshaw affected the calculated skin friction by less than 2%. Skin friction measurements usually agreed to within ±10% for the three tube diameters used except in the last half of the diffuser, where the value of d^* was low (50-60 for the 0.021-in. or 0.053-cm Preston tube).

Symmetry of the flow was checked at several locations by comparing the static wall pressures around the circumference of the flow at two cross sections and also by comparing several total pressure profiles made at the diffuser exit plane. Static wall pressures at the same cross section were found to be uniform circumferentially to within ±0.1 in. (0.25 cm).

IV. Experimental Results

Thrust values were obtained from the suspended thrust augmentor platform. Measurements were made of the combined augmentor system T_{aug}, the nozzle alone T_n, and the duct T_{duct}; however, no measurements of T_{aug} and T_{duct} were made for the throttled mode because of the dominating influence of screen drag. A value for ϕ of 1.45 was determined for test case A. If the experimental value of T_{aug} were divided by the theoretical value of T_n corresponding to one-dimensional choked, isentropic expansion to ambient pressure, the value of ϕ would be 1.392. Comparisons were made (Table 1) of the measured and isentropic values of the nozzle thrust and primary mass flow.

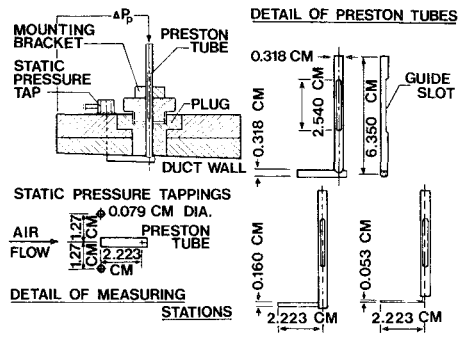

Fig. 4 Determination of skin friction using Preston tubes.

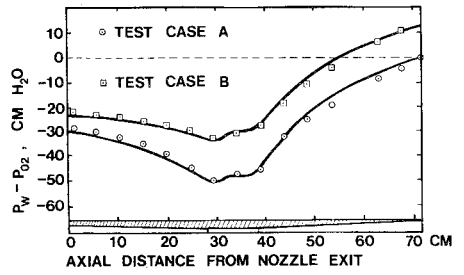

Fig. 5 Axial variation of static pressure.

Figures 5 and 6 show the axial variation of wall pressure for the augmentor inlet and duct section. The curves on Fig. 5 are the results of theoretical calculations, which will be discussed subsequently. A comparison can be made between the measured duct thrust T_{duct} and the thrust T''_{duct} obtained by integrating the wall pressure distributions. Measured duct thrust includes the net force acting on the inlet section. Figure 7 shows the wall pressure plotted against the radius squared. By integrating the plotted area representing the pressure contribution, the total axial thrust T''_{duct} can be calculated using

$$T''_{duct} = \pi(\bar{P}_w - P_{atm})\,dR_s^2 = 5.95\ \text{lbf}\ (26.5\ \text{N})$$

in which $(\bar{P}_w - P_{atm})$ is the difference between the wall pressure and atmospheric pressure (psia), and R_s is the local duct radius (in.). The flow model had predicted a skin friction

Table 1 Flow measurements

Test		Case A	Case B
Primary stagnation conditions	P_{01}	2.10 bar	2.11 bar
	T_{01}	27.3°C	26.1°C
Secondary stagnation conditions	P_{02}	1.004 bar	1.019 bar
	T_{02}	28.9°C	23.9°C
Mass flow rates	$\dot{m}_1$	0.123 kg/sec	0.123 kg/sec
		0.707 kg/sec	0.606 kg/sec
	$\dot{m}_2$	±2.5%	±2.5%
	$\dot{m}_2/\dot{m}_1$	5.71	4.92
Thrust values	T_{aug}	59.5 N	–
	T_n	41.1 N	41.1 N
	T_{duct}	23.9 N	–
Calculated duct thrust	T'_{duct}	24.5 N	–
Thrust and nozzle coefficients	Φ	1.45	–
	η_T	0.960	0.963
	$\eta_{\dot{m}}$	0.991	0.982

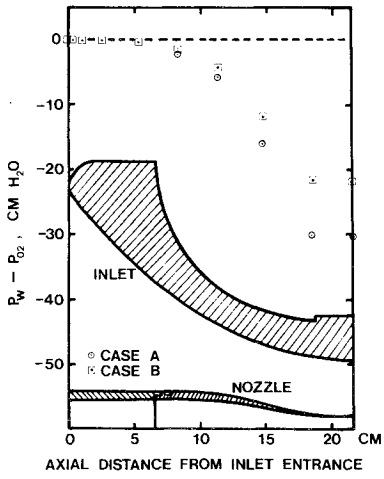

Fig. 6 Axial variation of wall static pressure for inlet section.

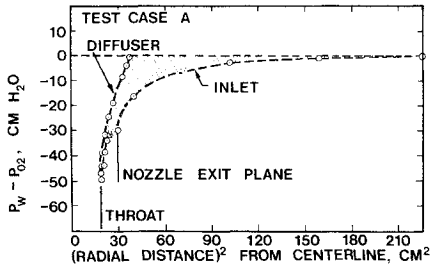

Fig. 7 Axial variation of wall static pressure.

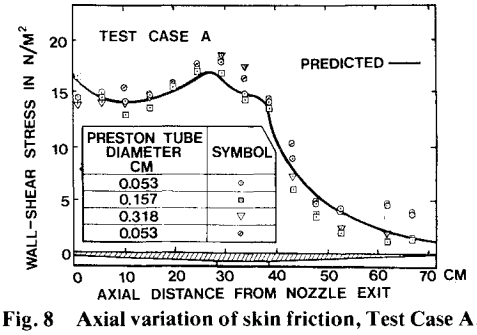

Fig. 8 Axial variation of skin friction, Test Case A.

drag of 0.45 lbf (2.00 N) for the duct section alone. Allowing for the drag force, the net duct thrust T'_{duct} was calculated as 5.50 lbf (24.5 N). The measured net thrust for the augmentor inlet and duct T_{duct} was found to be 5.38 lbf (23.9 N).

Three sizes of Preston tubes were used for the first test case, whereas only the two smaller tubes were used for test case B. Figures 8 and 9 show the results of the measurements made. Values of shear stress were obtained from the Bradshaw correlation. Agreement between different determinations of the skin friction for the Preston tubes can be noticed in the first two sections of the duct, even though the Preston tube diameters were not small compared to the boundary-layer thickness in the converging section of the duct. Larger discrepancies can be noticed in the diffuser. Differences in shear stress determinations were generally between the smallest diameter of Preston tube (0.21 in. or 0.53 cm) and the large tube(s). Low values of d^* (50-90) were found for the smallest tube in the diffuser, whereas d^* for the other tubes were well within the calibration limit as set by Bradshaw ($50 < d^* < 1000$).

Figure 8 illustrates the degree of repeatability of the shear stress measurements, made in different tests with approximately the same flow conditions. It appears that shear stress measurements are accurate to within $\pm 10\%$, except in regions where the shear stress is low, i.e., near the separation region.

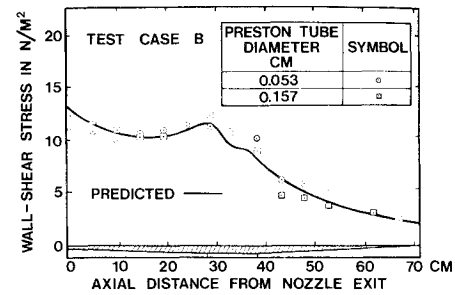

Fig. 9 Axial variation of skin friction, Test Case B.

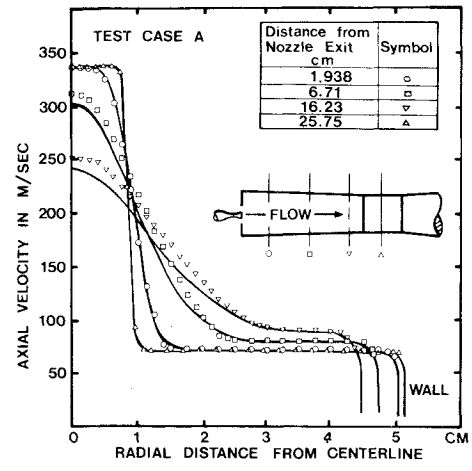

Fig. 10 Radial variation of axial velocity; data are from the converging and throat sections.

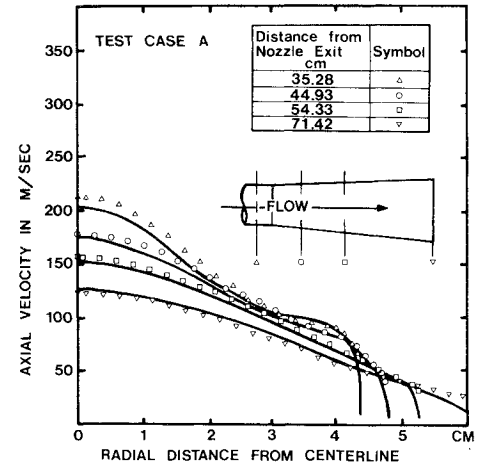

Fig. 11 Radial variation of axial velocity; data are from the throat and diffuser sections.

Figures 10-13 show the results of velocity measurements, as well as the results of theoretical calculations, which will be discussed subsequently. The velocity in the jet at the nozzle exit was approximately uniform, as was the velocity in the secondary stream. Wall boundary-layer thickness was small in the converging section of the duct. The jet and boundary-layer zones merge at a distance downstream of the nozzle between 9 and 10 in. (23-30 cm) for both test series. At the furthest downstream station, the flow velocity was quite nonuniform, although there was no evidence of flow separation.

V. Theoretical Calculations

The flow model used in these calculations is essentially the same as described by Hedges and Hill,[15] except that it employs viscosity rather than mixing length distributions to estimate shear stress. The method employs the boundary-layer

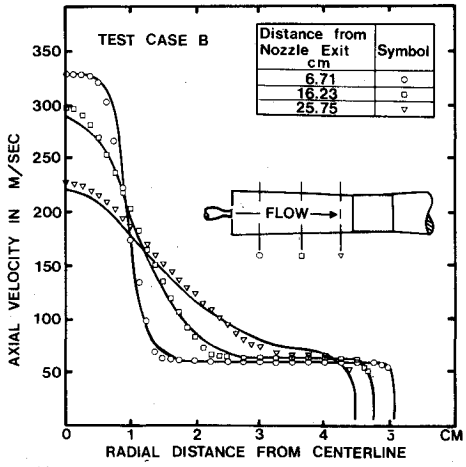

Fig. 12 Radial variation of axial velocity; data are from the converging section.

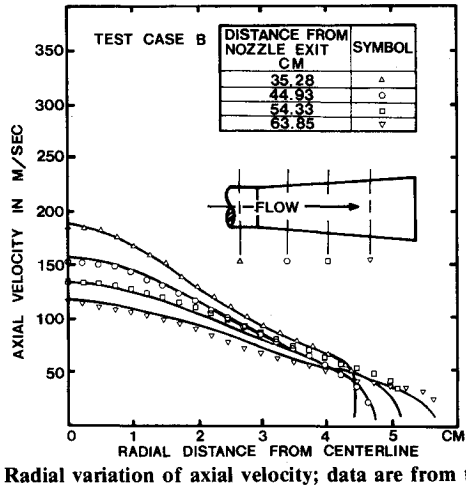

Fig. 13 Radial variation of axial velocity; data are from the throat and diffuser sections.

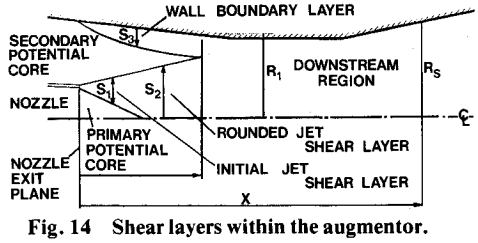

Fig. 14 Shear layers within the augmentor.

equations for subsonic compressible flow, transformed to streamline coordinates. The differential equations then are expressed in implicit finite-difference form for solution by a marching procedure from the nozzle exit plane. The initial conditions are determined at the nozzle exit plane from given primary and secondary mass flows and stagnation conditions, neglecting upstream losses. The velocity and temperature distributions at each step are determined from values at the previous step and the finite-difference form of the momentum equation, assuming an average pressure gradient for the step. The solution for each step requires a few iterations to satisfy continuity, thereby determining the pressure gradient and initial conditions for the next step.

The method of prescribing the eddy viscosity distributions will be described with the aid of Fig. 14. For each zone of the flow, an empirical relationship between eddy viscosity and shear layer width and velocity differential is specified. These relationships were adjusted so that calculations of centerline velocity, wall pressure, and wall shear stress would suit the data for case A. Then the same relationships were used in calculations for case B.

A. Jet Shear Layer

Here, the eddy viscosity was calculated from

$$\nu_T = 0.0068(U_\ell - U_2)\delta_j[1+2.0(U_2/U_\ell)]f_c \qquad (2)$$

in which δ_j is the jet shear layer width (either δ_1 or δ_2 in Fig. 14) and f_c is the compressibility factor due to Donaldson and Gray.[17] The factor in brackets in Eq. (2) is an approximate correction for the effect of the outer stream on the eddy viscosity of a free shear layer or jet.

B. Wall Boundary Layer

In the inner region of the boundary layer, the eddy viscosity was calculated from the following formula derived by Mellor [18]

$$\nu_T = [\xi^4/(\xi^3+6.9^3)] \qquad (3)$$

in which

$$\xi = K(\Delta y\sqrt{\tau/\rho}/\nu)$$

The von Karman constant K was set at 0.41.

In the outer region of the flow, the eddy viscosity was evaluated from the following form, which is also due to Mellor.[18]

$$\nu_T = 0.016U_2\delta^* \qquad (4)$$

with δ^* being the boundary-layer displacement thickness. Equation (3) is used for calculating ν_T everywhere in the boundary layer except where Eq. (4) provides a smaller value, in which case this latter value of ν_T is used. Since in most augmentor flows the value of δ^* in the wall boundary-layer region is thin, correction of these formulas for the effects of pressure gradient was not attempted.

C. Downstream Region

For this region of the flow, the inner zone (next to the wall) was treated again with the aid of Eq. (3). However, in accordance with a remark of Galbraith and Head[19] that the von Karman "constant" K could be as large as 0.76 in adverse pressure gradients, K was allowed to vary with pressure gradient in the following way.

$$K = 0.41[1+0.005(R/\tau_w)(dP/dx)] \qquad (5)$$

For the outer zone, the eddy viscosity was determined using

$$\nu_T = 0.0060[1+(R/\rho U_\ell{}^2)(dP/dx)]f_r$$

$$f_r = 1, \quad 0<y/R<0.3$$

$$f_r = 1-C[(y/R)-0.3], \quad 0.3<y/R<1$$

in which $C=0.340/(\delta^*/R)^{1.25}$, and δ^* is calculated at the end of the upstream region using

$$\delta_1{}^* = R-\left[2\int_0^R \frac{U}{U_\ell}y\,dy\right]^{1/2}$$

To avoid an abrupt transition between the eddy viscosity calculations for the upstream regions, an arbitrary transition distance of 5 diam was established within which the eddy viscosity distribution was calculated from

$$\nu_T = \nu_{TI}+[\nu_{TII}-\nu_{TI}][(x-x_I)/5D_I]$$

Table 2 Comparison of calculated and measured values

Test		Case A		Case B	
		Experimental	Calculated	Experimental	Calculated
Mass flow rates	$\dot{m}_1$	0.121 kg/sec	0.121 kg/sec	0.121 kg/sec	0.121 kg/sec
	$\dot{m}_2$	0.707 kg/sec	0.695 kg/sec	0.606 kg/sec	0.619 kg/sec
Thrust values	T_{aug}	59.56 N	62.8 N	–	–
	T_{II}	41.10 N	–	–	–
	T_{duct}	23.93 N	–	–	–
Thrust coefficient	Φ	1.450	1.53	–	–
Wall pressure at diffuser exit	$p_w - p_{t1}$	0	−0.03 cm H_2O	12.5 cm H_2O	11.7 cm H_2O

where

ν_{TI} = eddy viscosity at the end of the upstream region
ν_{TII} = eddy viscosity in the downstream region
x_I = axial distance at the end of the upstream region
D_I = duct diameter at the end of the upstream region

VI. Discussion of Results

Table 2 shows a comparison of experimental and calculated values of mass flow and thrust. As explained earlier, the secondary flow (obtained by integration of total pressure tube readings) is thought to be known to within ±2.5%. Using a calculated value of the mass flow rate quite near the mean of the experimental values (which were obtained at various streamwise stations) for case A leads to an exit pressure indistinguishably close to atmospheric pressure on the scale of Fig. 5. For the flow rates cited in Table 2 and the stagnation conditions given in Table 1, the computer program calculated a thrust of 14.5 lbf (64.45 N), but this calculation ignores losses upstream of the nozzle exit plane. Thrust loss in the nozzle can be inferred from the measured nozzle thrust coefficient given in Table 1, $\eta_T = 0.96$ for a nozzle thrust of 41.1 N. Subtracting the nozzle thrust loss of 0.04×41.1 N leads to the calculated augmentor thrust of 62.8 N shown in Table 2. This value is about 5% higher than the measured augmentor thrust. In the throttled exit test, thrust was not measured, but using the input primary and secondary mass flows shows that the exit pressure was very close to the calculated value (see Fig. 5).

Figures 5 and 8-13 show that, with the eddy viscosity formulas prescribed, it was possible simultaneously to fit wall pressure, shear stress, and velocity profile data quite closely. Figure 5 suggests that even the wall pressure distributions near the throat are followed closely by the calculation model. Figures 8 and 9 suggest that wall shear stresses are being calculated within experimental uncertainty, and that attempting to design short thrust augmentors according to a flow separation criterion is realistic. Figures 10-13 indicate good agreement between measured and predicted velocity profiles, although there are small discrepancies in the centerline region, and the wall boundary layer was too thin to observe with the probles used.

With this degree of agreement between calculated and observed wall shear, pressure, and velocity data, it is perhaps surprising that the calculated thrust is 5% high, even correcting for the nozzle thrust loss. We have not been able to show why this is so and doubt that the discrepancy is all due to losses in the inlet secondary flow.

The eddy viscosity prescription, including what appeared to be necessary corrections for the effect of pressure gradients and for a relaxation zone between the upstream and downstream regions, strikes us as unfortunately complex. One would hope that ultimately a simpler yet equally accurate prescription could be formulated.

VII. Conclusions

1) Detailed experimental data on an axisymmetric thrust augmentor confirm the validity of a finite-difference flow calculation method for predicting the flowfield and thrust augmentation. The theoretical calculation method is strongly dependent on the method of specifying the eddy viscosity distribution. Matching of flowfield data to calculation results by use of pressure-gradient-dependent eddy viscosity correlations led to close agreement with pressure, velocity, shear stress, and thrust data in the two flows tests. The augmentor thrust was predicted within about 5%.

2) The Preston tube provides a useful indication of augmentor flowfield behavior and is a valuable supplement to velocity and pressure field data in development of a turbulent flow model.

3) Although wall shear stress in the neighborhood of separation in the downstream part of the diffuser is difficult both to measure and to predict, it appears that the flow model is capable of reasonably good prediction of nearly separating flows (although it fails at the point of separation). It therefore appears capable of determining optimum geometry for short axisymmetric diffusers and for evaluating friction losses and thrusts of various axisymmetric designs.

Acknowledgment

The authors are grateful to the National Research Council of Canada for financial support for this work and to G. F. Marsters, D. Whittley, D. Garland, J. Farbridge, and J. Harris for many helpful conversations during the course of this project.

References

[1]Whittley, D. C., "Ejector-Powered Lift Systems of V/STOL Aircraft," *Canadian Aeronautics and Space Journal*, Vol. 20, May 1974, p. 179.

[2]Cheng, D. Y., Wang, P., and Chisel, D. M., "Experimental Study in Optimization," *Journal of Aircraft*, Vol. 10, Sept. 1973, pp. 569-570.

[3]Fancher, R. B., "Low-Area-Ratio, Thrust Augmenting Ejectors," *Journal of Aircraft*, Vol. 9, March 1972, pp. 243-248.

[4]Quinn, B., "Compact Ejector Thrust Augmentation," *Journal of Aircraft*, Vol. 10, Aug. 1973, pp. 481-486.

[5]Skoblenick, H. R., "Axisymmetric Thrust Augmentor Study," M.Sc. Thesis, Queen's University, Kingston, Ont., Canada, Dec. 1975.

[6]Mikhail, S., "Mixing of Co-Axial Streams Inside a Closed Conduit," *Journal of Mechanical Engineering Science*, Vol. 1 Jan. 1960, p. 50.

[7]Becker, H. A., "Concentration Fluctuations in Ducted Jet-Mixing," Ph.D. Thesis, Massachusetts Inst. of Technology, Dept. of Chemical Engineering, Aug. 1961.

[8]Cruse, R. E. and Tontoni, R., "Research in Co-Axial Jet-Mixing," Convair TR 62-354A, ASTIA A.D. 298 612, Nov. 1962, pp. 122-827.

[9]Curtet, R., "Confined Jets and Recirculation Phenomena with Cold Air," *Combustion and Flame*, Vol. 2, Dec. 1958, pp. 383-411.

[10]Razinsky, E. and Brighton, J. A., "Confined Jets Mixing for Non-Separating Conditions," *Journal of Basic Engineering*, Ser. D, Vol. 94, Sept. 1972, p. 551.

[11]Minner, G. L., "A Study of Axisymmetric, Incompressible, Ducted Jet Entrainment," Ph.D. Thesis, Purdue Univ., Jan. 1970.

[12]Hickman, K. E., Hill, P. E., and Gilbert, G. B., "Analysis and Testing of Compressible Flow Ejectors with Variable Area Mixing Tubes," *Journal of Basic Engineering*, Ser. D, Vol. 94 June 1972.

[13]Hedges, K. R., "Compressible Jet Mixing in Converging-diverging Axisymmetric Ducts," Ph.D. Thesis, Queen's Univ. at Kingston, Ont., Canada, 1973, pp.407-416.

[14]Hill, P. G., "Incompressible Jet Mixing in Converging-Diverging Axisymmetric Ducts," *Journal of Basic Engineering*, Ser. D, Vol. 89, March 1967, pp. 210-220.

[15]Hedges, K. R. and Hill, P. G., "Compressible Flow Ejectors – Parts I and II," *Journal of Fluids Engineering*, Vol. 96 Sept. 1974, pp. 272-281.

[16]Bradshaw, P. and Unsworth, K., "A Note on Preston Tube Calibrations in Compressible Flow," Imperial College Aero. Rept. 73-07, Sept. 1973.

[17]Donaldson, C. du P. and Grey, K. E., "Investigation of Free Sinking of Dissimilar Gases," *AIAA Journal*, Vol. 4, Nov. 1966, pp. 2017-2025.

[18]Mellor, G. L., "Incompressible Turbulent Boundary Layers with Arbitrary Pressure Gradients and Converging or Diverging Flows," *AIAA Journal*, Vol. 5, Sept. 1967, p. 1570.

[19]Galbraith, R. A. McD. and Head, M. R., "Eddy Viscosity and Mixing Length from Measured Boundary Layer Developments," *Aeronautical Quarterly*, May 1975, p. 331.